sustainability

MDPI

Article

Accident Trend Prediction of Heavy Metal Pollution in the Heshangshan Drinking Water Source Area Based on Integrating a Two-Dimensional Water Quality Model and GIS

Xiaowen Ding [1,2,*] and Ping Fang [1]

1 MOE Key Laboratory of Resources and Environmental System Optimization, College of Environmental Science and Engineering, North China Electric Power University, Beijing 102206, China
2 Hebei Key Laboratory of Power Plant Flue Gas Multi-Pollutants Control, Department of Environmental Science and Engineering, North China Electric Power University, Baoding 071003, China
* Correspondence: xiaowending@ncepu.edu.cn; Tel.: +86-010-61772982

Received: 25 June 2019; Accepted: 9 July 2019; Published: 24 July 2019

Abstract: In recent years, water pollution accidents have frequently occurred, which have caused enormous economic loss and an adverse social impact. In this study, an accident trend prediction system was developed based on integrating a two-dimensional water quality model and GIS, and Arsenic (As) was adopted as a typical pollutant to study the temporal-spatial changes of heavy metal pollutions under different hydrological and meteorological conditions in the Heshangshan drinking water source area. The simulation for a recent accident indicated that pollutant changes were influenced by lateral diffusion, longitudinal diffusion, flow velocity, water flow, and the self-purification of the water body. It took 79.5 min for the As concentration to meet the water quality standard during the dry period, while it spent 61.3 min, 71 min, and 52 min in the impound period, falling period, and flood period, respectively. The emergency response times were 32 min (in the flood period), 38 min (in the impound period), 48 min (in the falling period), and 52 min (in the dry period). Furthermore, wind speed and wind direction also had impacts on pollutant spread. The times in which the maximum values met the water quality standard were 71 min (southeast wind), 77 min (southwest wind), and 87 min (no wind). The emergency response times were 38 min (southeast wind), 49 min (southwest wind), and 59 min (no wind). This study not only provides a reference for relevant departments and managers to carry out a risk assessment, disaster prevention, and emergency management after actual pollution accidents, but also makes up for the lack of research on the spatial-temporal change of heavy metal pollutants.

Keywords: accident trend prediction system; heavy metal pollution; two-dimensional water quality model; GIS

1. Introduction

With the development of society, water resources play a crucial role in social and economical construction, and they are becoming a promotion or constraint factor for economic growth [1]. Through analyzing water pollution accidents in recent years [2,3], it was found that environmental pollution accidents have happened in many countries, such as China [4–6], the United States [7], and Japan [8]. For example, the Tuojiang river in the Sichuan province was polluted by a high concentration of ammonia nitrogen in 2004 [9]; in March 2011, the Fukushima nuclear accident was triggered by an earthquake and tsunami, which caused many radioactive substances to be deposited into the Pacific Ocean [10]; and the world's first major supertanker disaster occurred in 1967, when the SS Torrey

Canyon oil spill caused a large amount of crude oil to enter the Cornish coast in the English Channel [11]. The Heshangshan Drinking Water Source Area (HDWSA) is one of the most important water sources in the Three Gorges Reservoir area, and it is also the only water supply for the Heshangshan water plant in Chongqing city. Moreover, the industrial enterprise's chemical leakage caused by sudden accidents, toxic and harmful substance leakage due to loading and unloading in docks, petroleum contaminant leakage during transportation, and the leakage of hazardous chemicals caused by traffic accidents may be heavy metal risk sources in the HDWSA. Therefore, it will threaten the water quality of the 1.1 km^2 surface area of the HWDSA and millions of local people if heavy metal pollution accidents happen. According to water quality monitoring data from 2013 to 2015, it could be found that As concentration showed an increasing trend year by year, and it had the characteristics of a low dosage, high toxicity, variable valence, and refractory degradation, and the human body absorbed it through drinking water and the food chain. Additionally, it damaged human metabolism and caused severe toxic effects on human health [12]. Therefore, the HDWSA was chosen as the research area and Arsenic (As) was considered as a typical heavy metal pollutant. Considering the importance of water resources security and the particularity of the geographical location of the HDWSA under the condition of frequent water pollution accidents, it has important value to predict accident trends of heavy metal pollution in HDWSA. Many methods have been developed to assess heavy metals, including sediment quality guidelines (SQGs) [13], the potential contamination index (Cp) [14], the enrichment factor (EF) [15], and the modified degree of contamination (mCd) [16]. These methods need to compare a large number of measured data with reference material, while GIS can use the method of spatial interpolation to estimate attribute values at unsampled sites in a study area [17]. In addition, accident trend prediction has aroused the interest of many researchers under the condition of frequent water pollution accidents, so many water pollution diffusion models and pieces of software have been developed. These models and software have fast calculation and flexible analysis advantages [18–24], while most of the current water quality models for simulating pollution accidents have complex structures and multiple parameters due to the uncertainty and complexity of water pollution accidents [25]. Therefore, these factors limit the application of current water quality models in the field of dealing with water pollution accidents in real emergency decision-making. Moreover, some models might not present visualized simulation results well, which can lead to the diffusion and distribution of pollutants not being clearly and ideally expressed. In recent years, scholars from countries all over the world have found that integrating GIS into water quality models can effectively solve the above problems [26–36]. Li et al. used the EFDC (Environmental Fluid Dynamics Code) and WASP (Water Quality Analysis Simulation Program) models to simulate the pollutant arrival time and concentration at various locations after water pollution accidents, and the accident influence scope could be displayed in real time in the form of animations on the GIS layer [37]. Wang et al. developed the experimental system of water quality simulation for water pollution accidents based on GIS and SD (system dynamics) model, and dynamically simulated the spatial-temporal change of nitrobenzene concentration under the Songhua River water pollution accident conditions [38]. Olivera et al. integrated GIS into the SWAT(soil and water assessment tool) model to get the simulation results of the watershed hydrological and distributed simulation methods of nutrition immigration in the Nette drainage area [39]. Zhang et al. studied the integration of one-dimensional and two-dimensional steady-state water quality models with GIS and used the GIS's graphical display function to realize a visual display of the water quality model simulation [40]. These studies showed that integrating GIS into water quality models significantly improved the visible result of water quality models. However, the above research mainly focused on the concentration variation of organic pollutants, while studies on heavy metals are relatively limited, and further improvements are needed in both technical methods and theories.

As an effective measure to mitigate this concern, this research focused on heavy metal (As), and integrated GIS into a two-dimensional water quality model to predict the water quality change trend for the scenario of a water pollution accident. Therefore, an accident trend prediction system has been developed based on a database, model-based system, GIS, and visual interface of TECPLOT. Then, the system has been applied to HDWSA to simulate the change trend of heavy metal pollution (As) under different hydrological (the dry period, the falling period, the impound period, and the flood period) and meteorological conditions (southwest wind, southeast wind, and no wind). This study is the first attempt to predict the accident trend of heavy metal (As) pollution based on integrating GIS into a two-dimensional water quality model, which will provide a reference for relative researchers to predict the accident trend of heavy metal pollutions in other drinking water sources of the Three Gorges Reservoir area. It can reflect the change law of heavy metal pollution and polluted ranges to make up for the lack of research on water quality models of heavy metal pollution. Moreover, it can predict spatial-temporal change trends of the heavy metal pollutants under different hydrological conditions and different meteorological conditions to provide active decision support for managers to deal with water pollution accidents in the HDWSA.

2. Materials and Methodology

2.1. Research Area

The HDWSA in the Jiulongpo district is located in the southwest of Chongqing, which is surrounded by the Yangtze River and the Jialing River, between the downstream area of the Xiangjiang Dam and the upstream area of the Three Gorges Dam. The HDWSA is a vital water source in the Three Gorges Reservoir area, with a length of 1100 m, a width of about 1000 m, and a coverage area of 1.1 km^2. The geographical location is shown in Figure 1.

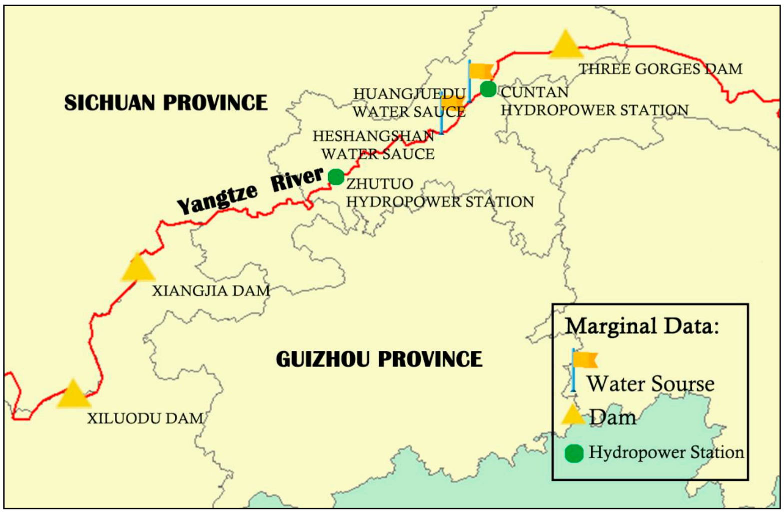

Figure 1. Positional relationship between the Heshangshan Drinking Water Source Area (HDWSA) and Xiangjia Dam and Three Gorges Dam.

The Heshangshan water plant belongs to the Jiulongpo district in Chongqing city, and it is the main plant that supplies water to urban residents. At present, the water supply capacity of the water plant is 300,000 t/d, which can provide water for 800,000 people, and the water supply scope mainly includes Yangjiaping, Daping, Shiqiaopu, and so on. The map of the HDWSA area is shown in Figure 2.

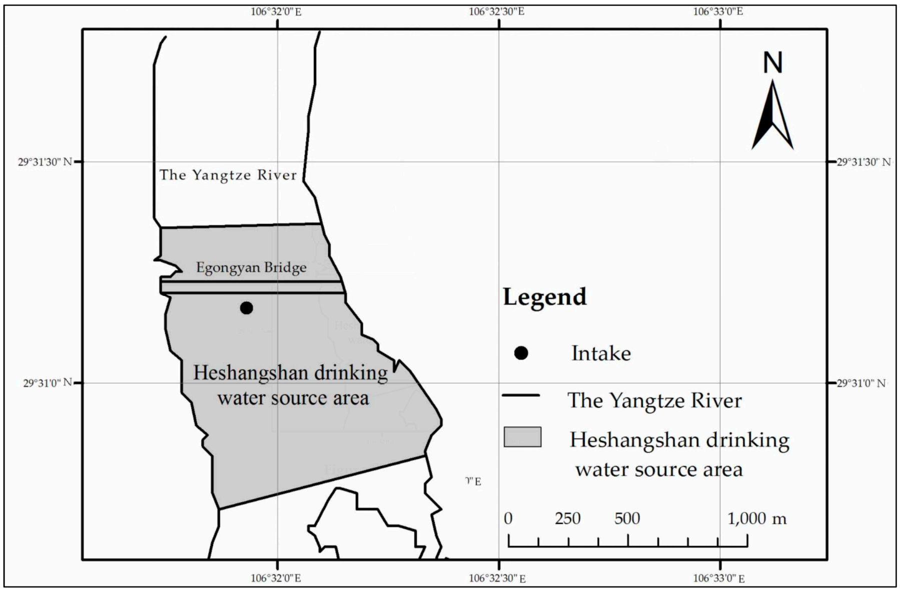

Figure 2. Location of the Heshangshan drinking water source area.

2.2. *Structure of the Accident Trend Prediction System*

The overall structure of the accident trend prediction system is shown in Figure 3. It includes four elements: a database, Two-dimensional Water Quality Model, GIS, and a visual interface of TECPLOT. Firstly, the user can set the boundary conditions and the relevant geographic information can be read from the database by GIS. Secondly, the fundamental mathematical models read these basic dates and execute the calculation commands based on the previous settings, and these calculation results can be found in the output database. Finally, these results can be displayed based on the visual interface of TECPLOT.

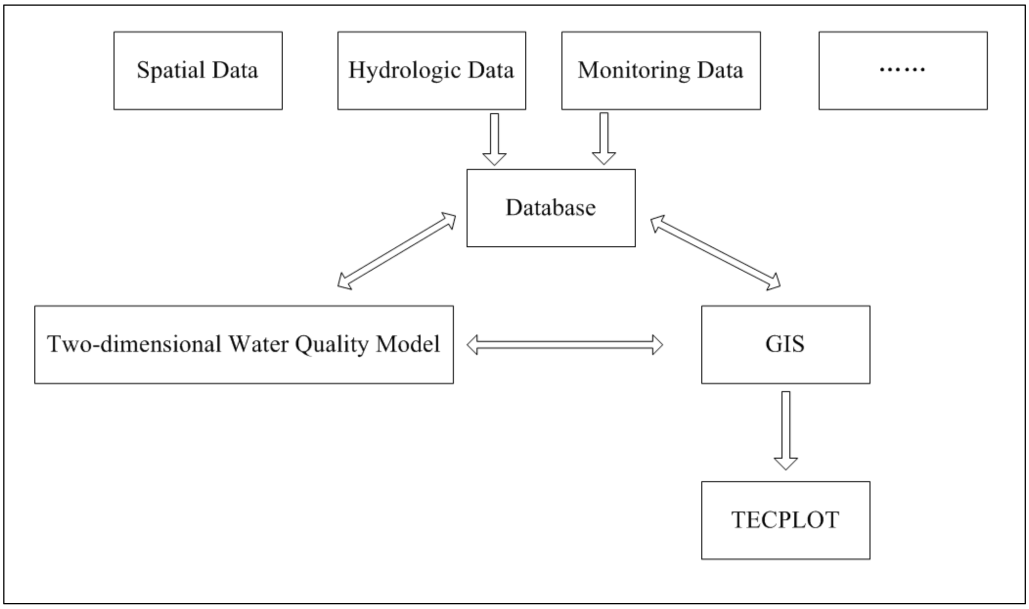

Figure 3. Structure of the accident trend prediction system.

2.3. Database

2.3.1. Boundary Conditions

In this research, based on the experience of other researchers when determining boundary conditions [41], the daily flow of the Zhutuo hydrological station was selected as the upstream boundary, and the water level of the Cuntan hydrological station was chosen as the downstream boundary. The daily flow of the Zhutuo hydrological station and the water level change of the Cuntan hydrological station in 2014 are shown in Figure 4. It could be seen clearly from this picture that the dry period occurred from November to March of the next year, the falling period occurred from April to June, the flood period occurred from June to September, and the impound period occurred in October. The upstream flow and the downstream water level during dry period, falling period, flood period, and impound period were 3974 m^3/s and 169.54 m, 5703 m^3/s and 163.74 m, 17,533 m^3/s and 173.06 m, and 10,400 m^3/s and 174.6 m, respectively.

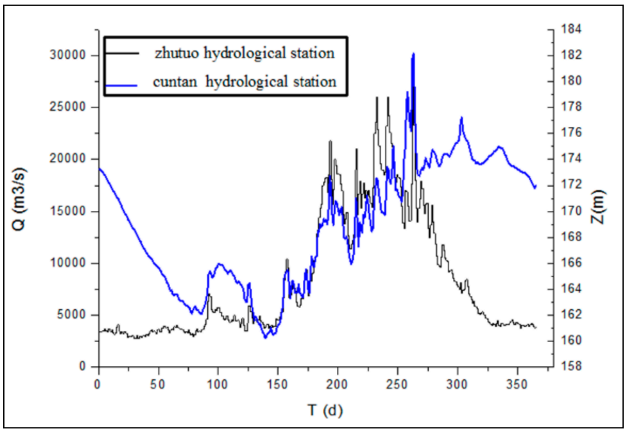

Figure 4. Daily flow and water level at the hydrological stations in 2014.

2.3.2. Initial Conditions

Considering that the water quality of HDWSA should meet the requirements of level III of the surface water environmental quality standard (GB3838-2002), the background concentration and initial concentration of As were 0.05 mg/L (level III) and 0 mg/L, respectively, under the hypothetical conditions. Moreover, the water intake was regarded as a sensitive point because of the residents' drinking water from the water intake.

2.4. Model Parameter Determination Method

The two-dimensional water quality model also needed to define the lateral diffusion coefficient and the longitudinal diffusion coefficient. The following empirical equation method was used to obtain the lateral diffusion coefficient, the longitudinal diffusion coefficient, the riverbed roughness rate, and the turbulent viscosity coefficient based on the research outputs of other researchers [42–45].

$$Ex = Kx\left(\frac{B}{h}\right)^{2.1}\left(\frac{u}{u_*}\right)^{0.7} hu_x, \tag{1}$$

$$Ey = Ki^{1.07}\frac{u^{0.48}}{u_*{}^{0.24}}\left(\frac{B}{h}\right)^{0.089}, \tag{2}$$

$$n = \frac{d_{0.65}^{1/6}}{19}, \tag{3}$$

$$Vt = \frac{\pi}{8} C_n u_x h, \tag{4}$$

Here, $u*$ (m/s) is the friction velocity; B (m) is the water surface width; u (m/s) is the average sectional velocity; h (m) is the average depth; i is the river slope; C (mg/L) is the concentration of simulated pollutant; u (m/s) is the velocity in the x directions; n is the roughness of the riverbed; Vt is the turbulent viscosity coefficient; and Ex and Ey are the diffusion coefficient in the x and y directions, respectively.

2.5. Basic Model System

2.5.1. Two-dimensional Water Quality Model

Through summarizing and analyzing simulation methods of heavy metal pollution accidents at home and abroad, it can be found that a three-dimensional simulation can produce a better simulation of heavy metal pollutant diffusion in natural rivers based on the mass conservation and continuity principles. However, the length of many rivers is generally several hundreds or thousands of kilometers, and the depth of many rivers is usually between several or dozens of meters. In addition, this research can ignore all water parameters in the water depth direction because most rivers belong to the shallow-wide category. Therefore, the three-dimensional water quality model was simplified to a two-dimensional water quality model by assuming that pollutants were thoroughly mixed in the water depth direction, and it was proved that the two-dimensional water quality model could accurately simulate the migration and transformation of heavy metal pollutants by comparing the current heavy metal water quality models [46,47]. After some reasonable assumptions and simplicity, these basic equations of heavy metal pollutants in rivers were obtained [48–51].

2D hydraulic equations:

$$\frac{\partial hv}{\partial t} + \frac{\partial hu}{\partial x} + \frac{\partial hv}{\partial y} = q, \tag{5}$$

$$\frac{\partial hu}{\partial t} + u\frac{\partial hu}{\partial x} + v\frac{\partial hu}{\partial y} = -g\frac{\partial h^2}{\partial x} - gh\frac{\partial h_b}{\partial x} - gn^2\frac{u\sqrt{u^2+v^2}}{h^{\frac{1}{3}}} + \frac{\partial}{\partial x}\left(\varepsilon_x h\frac{\partial u}{\partial x}\right) + \frac{\partial}{\partial y}\left(\varepsilon_x h\frac{\partial u}{\partial y}\right), \tag{6}$$

$$\frac{\partial hV}{\partial t} + u\frac{\partial hV}{\partial x} + v\frac{\partial hV}{\partial y} = -g\frac{\partial h^2}{\partial x} - gh\frac{\partial h_b}{\partial x} - gn^2\frac{V\sqrt{u^2+v^2}}{h^{\frac{1}{3}}} + \frac{\partial}{\partial x}\left(\varepsilon_y h\frac{\partial v}{\partial x}\right) + \frac{\partial}{\partial y}\left(\varepsilon_y h\frac{\partial v}{\partial y}\right), \tag{7}$$

2D water quality equations:

$$\frac{\partial hc}{\partial t} + u\frac{\partial hc}{\partial x} + v\frac{\partial hc}{\partial y} = \frac{\partial}{\partial x}\left(E_x\frac{\partial hc}{\partial x}\right) + \frac{\partial}{\partial y}\left(E_y\frac{\partial hc}{\partial y}\right) + H\sum S_i, \tag{8}$$

In the equations, x (m) is the river longitudinal flow distance; y (m) is the river transverse flow distance; u (m/s) and v (m/s) represent the velocity components in x and y directions, respectively; t (s) is the time; h (m) represents the river depth; H(m) is the river bottom elevation; c (mg/L) is the concentration of pollutants; ε_x (m^2/s) and ε_y (m^2/s) are the eddy viscosity coefficients in x and y directions, respectively; g (m^2/s) is the gravity; Ex (m^2/s) and Ey (m^2/s) are the diffusion coefficient in x and y directions, respectively; n is the roughness; q is the interval inflow (m^2/s); and Si (g/s) is the representative sink term.

2.5.2. Discretization Mathematical Model of Water Quality

The two-dimensional water quality model of Equation (4) could be solved based on the Finite Volume Method (FVM). The FVM has the advantages of a smaller size of computer memory and a faster calculating speed when compared with other calculation methods. Equation (9) [52] is a discrete equation, and the equation dispersion coefficients are shown in Table 1.

$$\alpha p\varnothing_p = \alpha_E\varnothing_E + \alpha_W\varnothing_W + \alpha_N\varnothing_N \tag{9}$$

Table 1. List of equation dispersion coefficients.

.	Continuity Equation	Momentum Equation	Water Quality Equation
ϕ	z'	$u\ v$	c
α_P	$\alpha_E + \alpha_W + \alpha_N + \alpha_S$	$(\alpha_E + \alpha_W + \alpha_N + \alpha_S + \alpha_p^0 - S_p\Delta x\Delta y)/\alpha$	
α_E	$\overline{d}_e h_e \Delta y$	$D_e A(\lvert P_e \rvert) + -F_e, 0$	
α_w	$\overline{d}_w h_w \Delta y$	$D_w A(\lvert P_w \rvert) + -F_w, 0$	
α_N	$\overline{d}_n h_n \Delta x$	$D_n A(\lvert P_n \rvert) + -F_n, 0$	
α_S	$\overline{d}_s h_s \Delta x$	$D_S A(\lvert P_S \rvert) + -F_S, 0$	
b	$u_e^* h_e \Delta y + u_w^* h_w \Delta y - v_n^* h_n \Delta x + v_s^* h_s \Delta x + \left(h_p^0 - h_p^*\right)\Delta x \Delta y/\Delta t + q\Delta x \Delta y$	$S_c\Delta x\Delta y + \phi_p^0 \alpha_p^0 + (1-\alpha)/\alpha\alpha_p u_p^*$	
α_p^0	-	$h_p^0 \Delta x\Delta y/\Delta t$	
D_e	-	$(\varepsilon_x h)_e \Delta y/\Delta x$	
P_e	-	F_e/D_e	
S_p	-	$-gn^2\sqrt{u^2+v^2}/h^{1/3} - q$	$-KH$
S_c	-	$-gh(Z_e - Z_w)/\Delta x$	$c_0 H$
u_e^*	$((\sum \alpha_{nb} u_{nb} + b)/\alpha_P)_e + (gh\Delta y/\alpha_P)_e (Z_P - Z_E)$	-	-
$\overline{d}_e$	$(\Delta y/\alpha_P)_P (\delta x)_{e^+}/(\delta x)_e + \left(\Delta y/\alpha_p\right)_E (\delta x)_{e^-}/(\delta x)_e$	-	-

2.5.3. Grid Division of Complex Boundaries

Since the boundary of natural channels is irregular, it is necessary to change the complex irregular regions into regular rectangular regions when solving the discrete numerical solution of the irregular region. It can be seen from the Equation (9) that the coefficient matrix of the discrete algebraic equations was a five-diagonal matrix, so it was solved by the tridiagonal matrix algorithm (TDMA) algorithm. The implementation process was as follows. First of all, the ϕ_E and ϕ_W obtained from the previous iteration were introduced into the discrete formula to artificially generate a tridiagonal matrix. Secondly, the ϕ_N and ϕ_S could be obtained by using the TDMA algorithm. Finally, the value of each layer was obtained by column-by-column scanning and continuous scanning until convergence. All of the above processes were repeated to transform the irregular topography of HDWSA into a regular rectangular area. The HDWSA was divided into 250 × 280 grid points and this result is shown in Figure 5 [53].

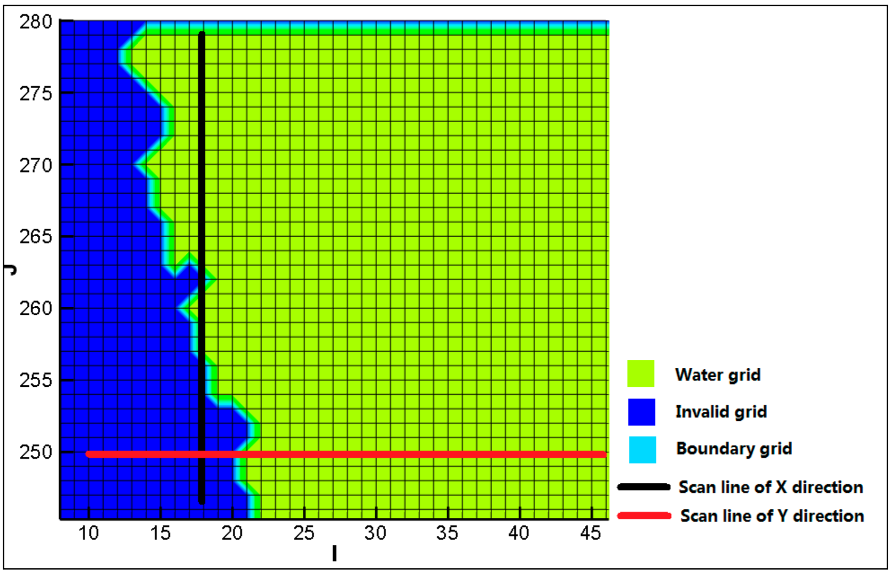

Figure 5. Schematic diagram of boundary and scan lines schematic.

2.5.4. Parameter Calibration

In order to verify the rationality and validity of the two-dimensional water quality model parameters, the roughness of the riverbed and the turbulent viscosity coefficient were calibrated by using the flow conditions (flow Q = 17,533 m^3/s, water level Z = 227.5 m) during the flood period in HDWSA. The riverbed roughness rate was n = 0.0854 [54] and the turbulent viscosity coefficient was Vt = 0.05 m^2/s [55] after calibration.

2.5.5. Model Verification

Through using the dry period hydrologic data (Q = 3974 m^3/s; Z = 169.54 m) in HDWSA, the accuracy of the lateral diffusion coefficient (0.1–2 m^2/s) and longitudinal diffusion coefficient (1–5 m^2/s) was verified by comparing the simulated values and the measured values of the As concentration [56–59]. After parameter calibration and verification, the maximum errors between the simulation results and the measured results were less than 20%, as Figure 6 shows, which indicated that the water flow and water quality of HDWSA could be well-simulated. In summary, this two-dimensional water quality model could be used as an accident trend prediction of heavy metal pollution in HDWSA.

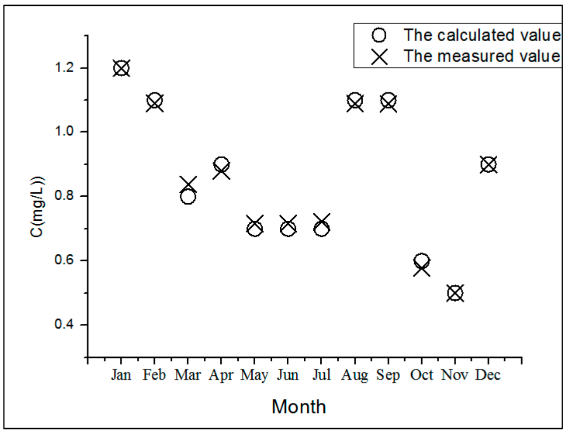

Figure 6. Map of simulated and observed values of Arsenic (As) concentration.

2.6. GIS

Through numerically classifying some attribute data of spatial information, the degree of pollution could be visualized by GIS and shown in different colors. The calculation result was automatically generated as the value of each corresponding discrete area by using the program, the visualization expression of simulation result was realized by using the rendering function of GIS, and these results could be displayed based on the visual interface of TECPLOT.

2.7. Model Application

2.7.1. Accident Source Design

Since heavy metal pollution accidents have not happened in recent years, this study used the hypothetical method to simulate the occurrence of As pollution accidents in the HDWSA based on risk source analysis and pollutions feature investigation. It was assumed that As pollutant leakage events occurred in the water source about 100 m upstream and it was discharged at a speed of 1000 kg/h for 10 min. The As pollutant degradation rate constant was k = 0 in reference to relevant data.

2.7.2. Accident Scenarios Design

Considering the uncertain characteristics of pollution accidents and the effects of different factors on pollutants, Scenario 1 and Scenario 2 were established respectively to predict the accident trend of heavy metal pollution (As) in different hydrologic and meteorological conditions. The purpose of Scenario 1 was to simulate As pollutant diffusion during the dry period, falling period, impound period, and flood period for exploring the influence of hydrologic factors on pollutants. In addition, Chongqing lies in the subtropical monsoon climate belt, with southwest wind prevailing in summer and southeast wind occuring in winter. In order to explore the effect of wind factors on pollutants, Scenario 2 was founded to simulated heavy metal pollutant (As) diffusion in a southwest wind condition, southeastern wind condition, and no wind condition.

3. Results and Discussion

The spatial-temporal distribution of the As pollutant in HDWSA was obtained through FORTUNE program simulation calculation, and the As pollutant spatial-temporal changes could be presented on the visual interface of TECPLOT.

3.1. *Simulation Results of Pollution Accident in Scenario 1*

3.1.1. Analysis of Pollutant Spatial-Temporal Changes

Figures 7–10 show the As pollutant spatial-temporal changes after a pollution accident that occurred at 20, 30, 40, and 50 min under the conditions of the dry period, falling period, impound period, and flood period, respectively. From these figures, it can be seen that the As pollutant diffused from the center to surrounding area after the accident and the high pollutant concentration area was closed to the pollutant emission point at this time. As time passed, the high-pollutant concentration area gradually moved away from the emission point, and the polluted ranges gradually expanded, which was because of the effects of lateral diffusion and longitudinal diffusion. The simulation results conform to the regular change of actual pollutants, so the method is accurate and reliabile.

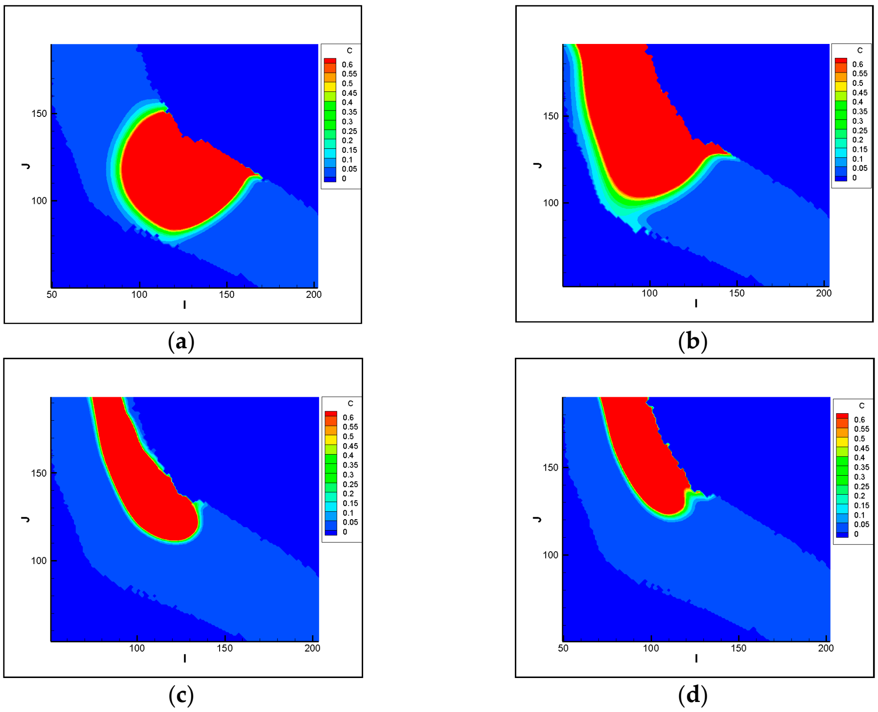

Figure 7. (**a**) The spatial-temporal changes of As pollutant after 20 min in the dry period; (**b**) the spatial-temporal changes of As pollutant after 30 min in the dry period; (**c**) the spatial-temporal changes of As pollutant after 40 min in the dry period; (**d**) the spatial-temporal changes of As pollutant after 50 min in the dry period.

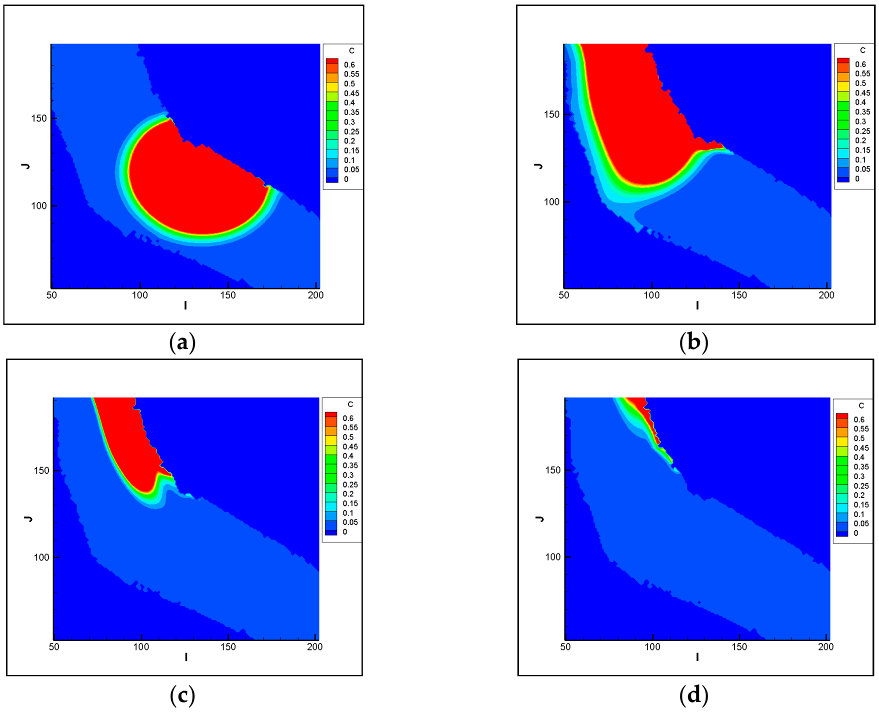

Figure 8. (**a**) The spatial-temporal changes of As pollutant after 20 min in the falling period; (**b**) the spatial-temporal changes of As pollutant after 30 min in the falling period; (**c**) the spatial-temporal changes of As pollutant after 40 min in the falling period; (**d**) the spatial-temporal changes of As pollutant after 50 min in the falling period.

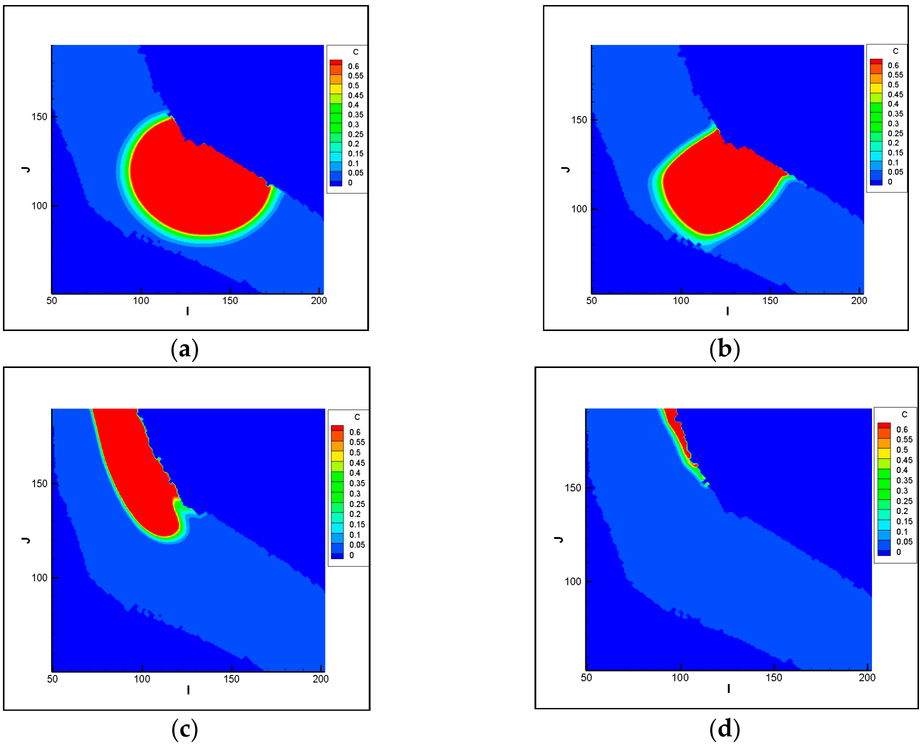

Figure 9. (**a**) The spatial-temporal changes of As pollutant after 20 min in the impound period; (**b**) the spatial-temporal changes of As pollutant after 30 min in the impound period; (**c**) the spatial-temporal changes of As pollutant after 40 min in the impound period; (**d**) the spatial-temporal changes of As pollutant after 50 min in the impound period.

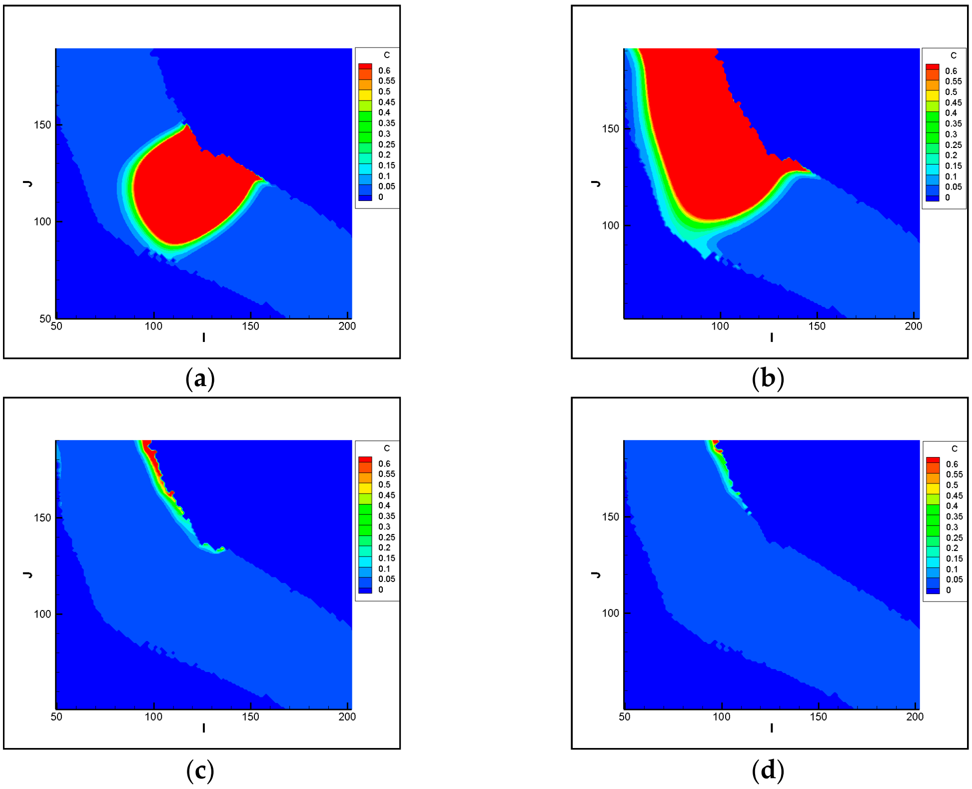

Figure 10. (**a**) The spatial-temporal changes of As pollutant after 20 min in the flood period; (**b**) the spatial-temporal changes of As pollutant after 30 min in the flood period; (**c**) the spatial-temporal changes of As pollutant after 40 min in the flood period; (**d**) the spatial-temporal changes of As pollutant after 50 min in the flood period.

3.1.2. Analysis of the Polluted Ranges

It can be seen from Figures 7–10 that the polluted ranges gradually increased when the As pollutant moved from upstream to downstream. The expansion of the polluted ranges was mainly caused by the lateral diffusion and longitudinal diffusion and was affected by flow speed. Through comparing pollution ranges under four different hydrologic conditions, it could be seen that the polluted ranges in the dry period were smaller than those for the other three periods and the flood period had the largest pollution ranges and the shortest residence time. Moreover, the polluted ranges in the impound period were larger than those of the dry period and falling period. The expansion of this phenomenon was due to the flow velocity during the flood period being larger than during the dry period, and the impound period having a greater water flow in comparison to the dry period and falling period. The results show that the flow velocity and water flow can influence polluted ranges and this has been confirmed by researchers [60].

3.1.3. The Change of Maximum Pollution Concentration

Figure 11 shows the changing trend of As maximum pollution concentration over time. It can be seen from this figure that the values of maximum pollutant concentration are higher than for the other three periods, which is consistent with the results of practical monitoring in 2014. The times at which the maximum values meet the water quality standard are 79.5 min (the dry period), 61.3 min (the impound period), 71 min (the falling period), and 52 min (the flood period). The results show that the migration speed of the As pollutant from fast to slow was in the flood period, impound period, falling period, and dry period. This is due to the flood period having an abundant water quantity and the fact that the As pollutant could spread rapidly under the action of water flow. Moreover, the migration and degradation of the heavy metal pollutant and self-purification of the river also affect the pollutant residence time [61].

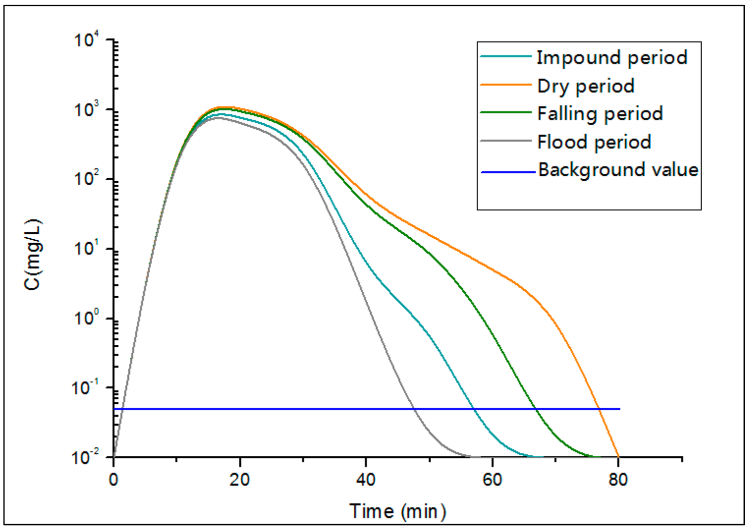

Figure 11. Change of the maximum concentration of Arsenic (As) contamination under different hydrological conditions.

3.1.4. Analysis of the Emergency Response Time

Figure 12 shows the pollution concentration change of the water intake of the HDWSA water plant over time under the conditions of the dry period, falling period, impound period, and flood period, respectively, and the values of emergency time when the As concentration was higher than the background value could be obtained. In the flood period, the water intake began to be influenced at 2 min after the accident and the pollutant passed the water intake at 34 min after the accident, and it can be shown that the emergency response time is 32 min (the flood period). In the same way, the emergency response times are 38 min (from 2 min to 40 min after the accident), 48 min (from 2 min to 50 min after the accident), and 52 min (from 2 min to 54 min after the accident) in the impound period, falling period, and dry period, respectively.

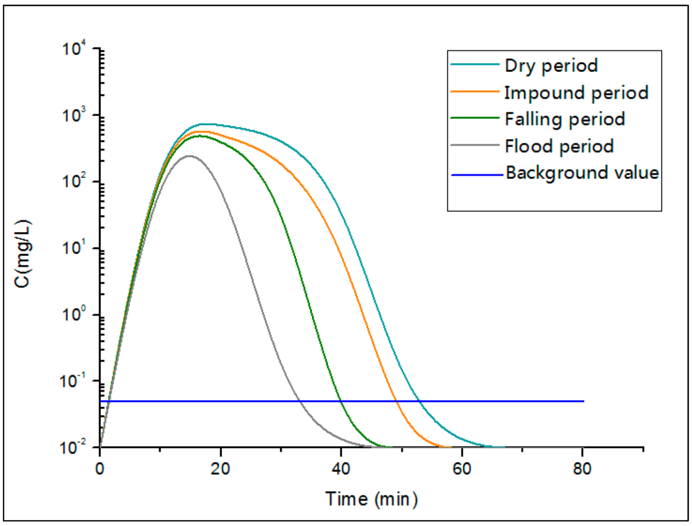

Figure 12. The pollution concentration change of the water intake under different hydrological conditions.

3.2. Simulation Results of the Pollution Accident in Scenario 2

3.2.1. Analysis of Pollutant Spatial-Temporal Changes

Figures 1–15 show As pollutant spatial-temporal changes in the falling period after the pollution accident occurred at 20 min, 30 min, 40 min, and 50 min under the conditions of southwest wind, southeast wind, and no wind. Through analyzing pollutant spatial-temporal changes under the three different meteorological conditions, it showed that As pollutant spread to the right bank of the water source area under the southeast wind and southwest wind conditions and As pollutant spread from its center to around under the condition of no wind. This is because wind speed affected the pollutant diffusion direction and made it spread to the shore.

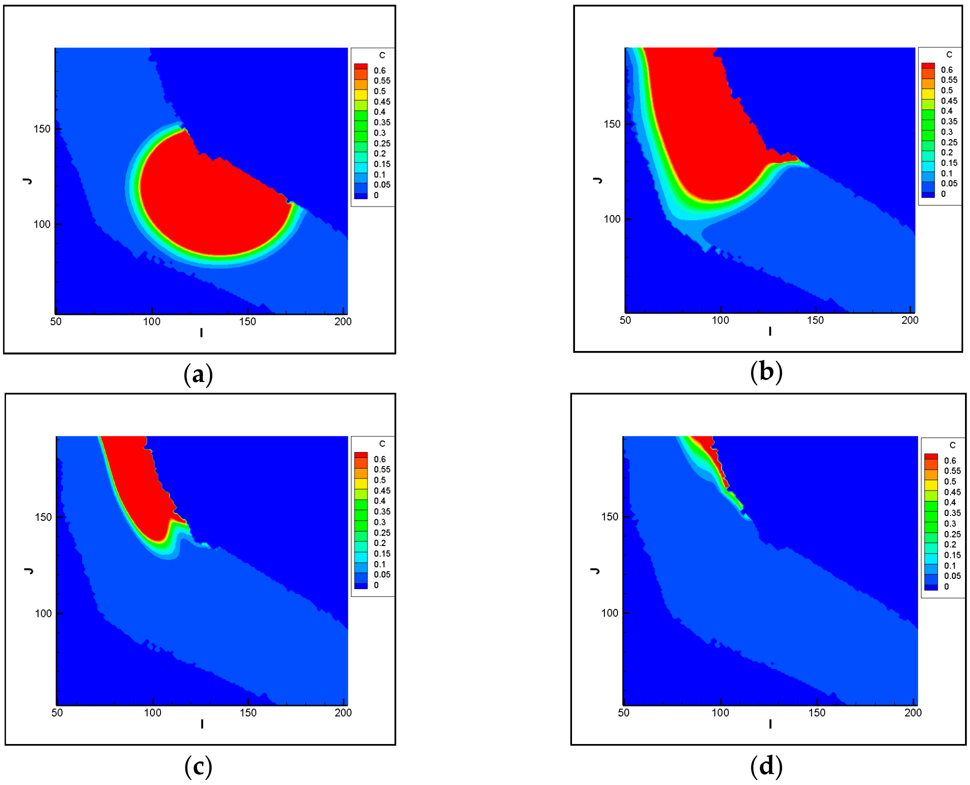

Figure 13. (**a**) The spatial-temporal changes of Arsenic (As) pollutant after 20 min in the southwest wind condition; (**b**) the spatial-temporal changes of As pollutant after 30 min in the southwest wind condition; (**c**) the spatial-temporal changes of As pollutant after 40 min in the southwest wind condition; (**d**) the spatial-temporal changes of As pollutant after 50 min in the southwest wind condition.

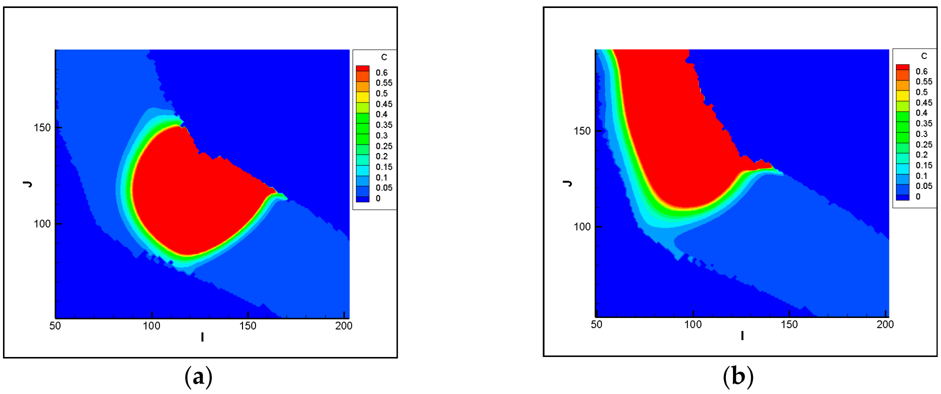

Figure 14. *Cont.*

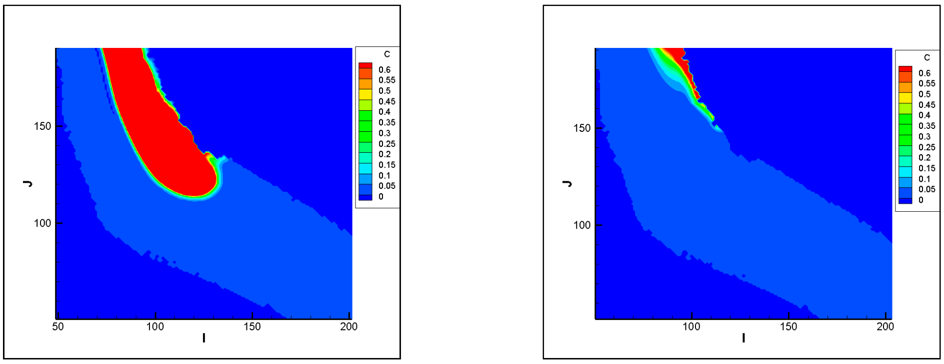

(**c**) (**d**)

Figure 14. (**a**) The spatial-temporal changes of As pollutant after 20 min in the southeast wind condition; (**b**) the spatial-temporal changes of As pollutant after 30 min in the southeast wind condition; (**c**) the spatial-temporal changes of As pollutant after 40 min in the southeast wind condition; (**d**) the spatial-temporal changes of As pollutant after 50 min in the southeast wind condition.

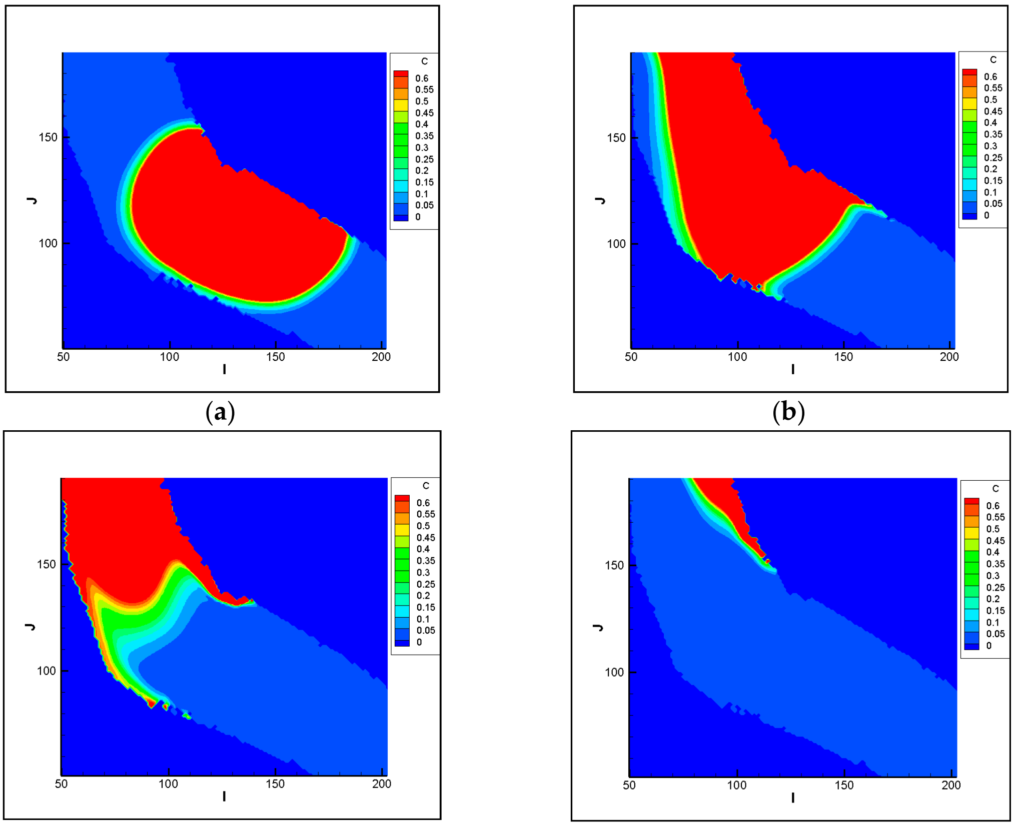

(**a**) (**b**)

(**c**) (**d**)

Figure 15. (**a**) The spatial-temporal changes of As pollutant after 20 min in the no wind condition; (**b**) the spatial-temporal changes of As pollutant after 30 min in the no wind condition; (**c**) the spatial-temporal changes of As pollutant after 40 min in the no wind condition; (**d**) the spatial-temporal changes of As pollutant after 50 min in the no wind condition.

3.2.2. Analysis of the Polluted Ranges

Through the comparison of polluted ranges under three different meteorological conditions, it can be found that the largest polluted area was the southeast wind condition and the smallest polluted area was the no wind condition. There are two expiations for this phenomenon; one reason for this is that the wind can increase the speed of water flow and another reason is that the southeast wind direction is consistent with the water direction, which is beneficial to the pollutant diffusion. Therefore, the polluted ranges have expanded.

3.2.3. Analysis of the change of Maximum Pollution Concentration

Figure 16 shows the change trends of the maximum pollution concentration over time under the meteorological conditions of southeast wind, southwest wind, and no wind. The times at which the maximum values meet the water quality standard are 71 min (the southeast wind), 77 min (the southwest wind), and 87 min (no wind). It could be seen from these results that the maximum pollution concentration decreased slowly under the southwest wind and no wind condition. The results indicate that the southwest wind and southeast wind are more conducive to pollutant diffusion than no wind, which is caused by the wind forces accelerating the pollutant diffusion, and the conclusion is consistent with Yu's results on the dispersion characteristics of pollutants in the Daning reservoir [62].

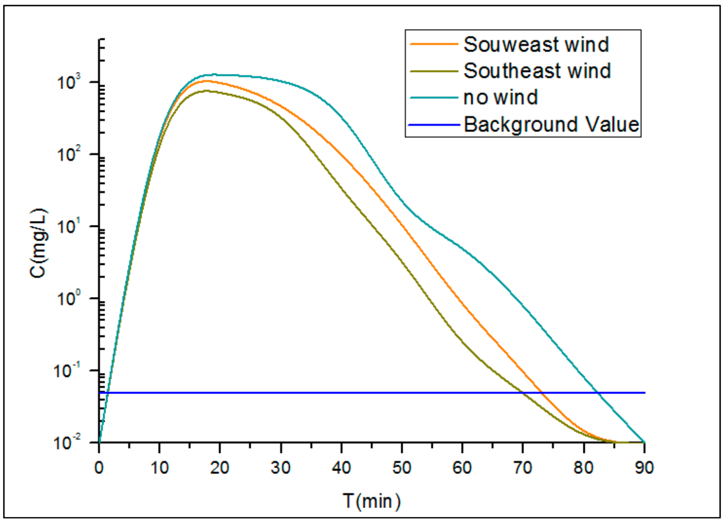

Figure 16. The change of the maximum concentration of Arsenic (As) pollutant under different meteorological conditions.

3.2.4. Analysis of the Emergency Response Time

Figure 17 shows the pollution concentration change trends of the water intake of the HDWSA water plant over time under the meteorological conditions of southeast wind, southwest wind, and no wind. It can be seen that the pollutants enter into the water intake at 2 min after the accident and the water intake eliminated dangers at 61 min after the accident under the no wind condition, so the conclusion can be drawn that the emergency response time is 59 min (no wind). In the same way, the emergency response times are 38 min (from 2 min to 40 min after the accident) and 49 min (from 2 min to 51 min after the accident) in terms of the southeast wind and southwest wind, respectively.

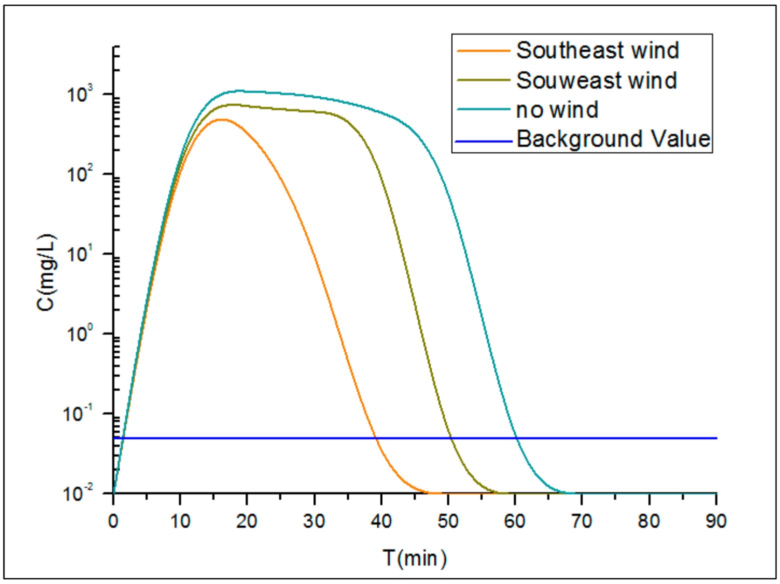

Figure 17. Pollution concentration change of the water intake under different meteorological conditions.

4. Conclusions

This research adopted GIS to explore the movement rule of heavy metal (As) and established an accident trend prediction system to predict an accident trend of heavy metal pollution (As) based on integrating a two-dimensional water quality model and GIS. Firstly, the two-dimensional water quality model was calibrated and verified based on the hydrological data in 2014, and the results showed that the model had a high accuracy and could be used to simulate heavy metal pollution (As). Secondly, the HDWSA was chosen as the research area and Arsenic (As) was considered as a typical heavy metal pollutant, and the temporal-spatial changes of heavy metal pollution under different hydrological conditions and different meteorological conditions were studied. Considering the influence of hydrological factors and wind factors, Scenario 1 was established to simulate the As pollutant changes in four different periods: dry period, falling period, impound period, and flood period. Additionally, Scenario 2 was founded to simulate heavy metal pollutant (As) diffusion in thesouthwest wind condition, southeastern wind condition, and no wind condition. Finally, through a series of analysis (analysis of pollution spatial-temporal changes, analysis of polluted ranges, analysis of maximum pollution concentration, and analysis of emergency response time) under different hydrologic conditions and different meteorological conditions, the effects of hydrological factors and wind factors on the changes of heavy metal pollution were discussed.

It could be found that different hydrological periods and different meteorological conditions have different impacts on the As pollutant migration and transformation process. In Scenario 1, it took 79.5 min for the maximum values to meet the water quality standard during the dry period, while it took 61.3 min, 71 min, and 52 min in the impound period, falling period, and flood period, respectively. The emergency response times were 32 min (from 2 min to 34 min after the accident), 38 min (from 2 min to 40 min after the accident), 48 min (from 2 min to 50 min after the accident), and 52 min (from 2 min to 54 min after the accident) in the flood period, impound period, falling period, and dry period respectively. This shows that the lateral diffusion, longitudinal diffusion, flow velocity, water flow, and water self-purification can affect pollutant diffusion speed and polluted ranges, so it is necessary to fully consider the different hydrodynamic conditions in actual pollution accidents to ensure the accuracy of emergency response times. In addition, it can be seen from the Scenario 2 results that the times at which the maximum values meet the water quality standard are 71 min (the southeast wind), 77 min (the southwest wind), and 87 min (no wind). The emergency response times are 59 min (from 2 min to 61 min after the accident), 38 min (from 2 min to 40 min after the accident), and 49 min (from 2 min to 51 min after the accident) under southeast wind and southwest wind conditions, respectively.

This showed that heavy metal pollution (As) became more easily diffused under the impact of wind force, and wind could affect the speed and direction of pollutant diffusion. Therefore, the influence of different meteorological conditions on pollutants should also be considered when dealing with actual pollution accidents to ensure the accuracy of emergency response times.

In conclusion, the method could be utilized to predict the accident trend of heavy metal pollution after water pollution accidents. This study is the first attempt to predict the accident trend of heavy metal (As) pollution based on integrating GIS into a two-dimensional water quality model. On the one hand, it reflects the change law of heavy metal pollution and polluted ranges to make up for the lack of research on water quality models of heavy metal pollution. On the other hand, it predicts the spatial-temporal change trend of heavy metal pollutants under different hydrological conditions and different meteorological conditions to establish proper emergency treatments to prevent the occurrence of crises and mitigate the harm of emergencies. This study provides a reference for researchers to predict the accident trend of heavy metal pollutions in other drinking water sources of the Three Gorges Reservoir area. Therefore, approaches for different heavy metals in other drinking water sources will be developed in the future.

Author Contributions: Formal analysis: X.D.; resources: X.D. and P.F.; investigation: P.F.; data curation: P.F.; writing—original draft: X.D.; writing—review and editing: P.F.

Funding: This research was funded by the Fundamental Research Funds for the Central Universities of PRC (2017YQ002) and the national key scientific and technological projects of the PRC (2014ZX07104-005).

Acknowledgments: We are very grateful to the national key scientific and technological projects of the PRC (2014ZX07104-005) and the Fundamental Research Funds for the Central Universities of PRC (2017YQ002). The authors gratefully acknowledge the financial support of the programs and agencies.

Conflicts of Interest: The authors declare no conflicts of interest.

References

1. Scheili, A.; Rodriguez, M.J.; Sadiq, R. Impact of human operational factors on drinking water quality in small systems: An exploratory analysis. *J. Clean. Prod.* **2016**, *133*, 681–690. [CrossRef]
2. Myeong, G.H.; Jeong, J.C. The Assessment of Water Pollution Accident on Dam watershed using GIS. *J. Environ. Impact Assess.* **2011**, *20*, 489–496.
3. Tang, C.H.; Yi, Y.J.; Yang, Z.F. Risk forecasting of pollution accidents based on an integrated Bayesian network and water quality model for the South to North Water Transfer Project. *Ecol. Eng.* **2016**, *96*, 109–116. [CrossRef]
4. Qu, J.H.; Meng, X.L.; Ye, X.Q. Characteristic variation and original analysis of emergent water source pollution accidents in China between 1985 and 2013. *Environ. Sci. Pollut. Res.* **2016**, *23*, 19675–19685. [CrossRef] [PubMed]
5. Liu, R.Z.; Zhang, K.; Zhang, Z.J.; Borthwick, A.G.L. Water-Scale Environmental Risk Assessment of Accident Water Pollution: The Case of Laoguan River, China. *J. Environ. Inform.* **2018**, *31*, 87–96.
6. Hou, Y.; Zhang, T. Evaluation of major polluting accidents in China—Results and perspectives. *J. Hazard. Mater.* **2009**, *168*, 670–673. [CrossRef] [PubMed]
7. Pulido-Velazquez, M.; Escriva-Bou, A. Developing a water-energy-GHG emissions modeling framework: Insights from an application to California's water system. *Environ. Model. Softw.* **2018**, *109*, 54–65.
8. Ueda, S.; Hasegawa, H.; Kakiuchi, H. Nuclear accident-derived H-3 in river water of Fukushima Prefecture during 2011–2014. *J. Environ. Radioact.* **2015**, *146*, 102–109. [CrossRef] [PubMed]
9. Xu, G.; Liu, J.; Hu, G. Distribution and source of organic matter in surface sediment from the muddy deposit along the Zhejiang coast, East China Sea. *Mar. Pollut. Bull.* **2017**, *123*, 325–399. [CrossRef] [PubMed]
10. Koo, Y.H.; Yang, Y.S.; Song, K.W. Radioactivity release from the Fukushima accident and its consequences: A review. *Prog. Nucl. Energy* **2014**, *74*, 61–70. [CrossRef]
11. Wells, P.G. The iconic Torrey Canyon oil spill of 1967-Marking its legacy. *Mar. Pollut. Bull.* **2017**, *115*, 1–2. [CrossRef] [PubMed]
12. Mohan, D.; Pittman, C.U. Arsenic removal from water/wastewater using adsorbents—A critical review. *J. Hazard. Mater.* **2007**, *142*, 1–53. [CrossRef] [PubMed]

13. MacDonald, D.D.; Ingersoll, C.G.; Berger, T.A. Development and evaluation of consensus-based sediment quality guideline for freshwater ecosystems. *Arch. Environ. Contam. Toxicol.* **2000**, *39*, 20–31. [CrossRef]
14. Dauvalter, V.; Rognerud, S. Heavy metal pollution in sediments of the Pasvik River drainage. *Chemosphere* **2001**, *42*, 9–18. [CrossRef]
15. Sakan, S.M.; Đorđević, D.S.; Manojlović, D.D.; Predrag, P.S. Assessment of heavy metal pollutants accumulation in the Tisza river sediments. *J. Environ. Manag.* **2009**, *90*, 3382–3390. [CrossRef] [PubMed]
16. Abrahim, G.M.S.; Parker, R.J. Assessment of heavy metal enrichment factors and the degree of contamination in marine sediments from Tamaki Estuary Auckland, New Zealand. *Environ. Monit. Assess.* **2008**, *136*, 227–238. [CrossRef]
17. Maanan, M.; Saddik, M.; Maanan, M.; Chaibi, M.; Assobhei, O.; Zourarah, B. Environmental and ecological risk assessment of heavy metals in sediments of Nador lagoon, Morocco. *Ecol. Indic.* **2015**, *48*, 616–626. [CrossRef]
18. Taylor, S.D.; He, Y.; Hiscock, K.M. Modeling the impacts of agricultural management practices on river water quality in eastern England. *J. Environ. Manag.* **2016**, *180*, 147–163. [CrossRef]
19. Shi, Y.; Xu, G.; Wang, Y.; Engel, B.A.; Peng, H.; Zhang, W. Modelling hydrology and water quality processes in the Pengxi River basin of the Three Gorges Reservoir using the soil and water assessment tool. *Agric. Water Manag.* **2017**, *182*, 24–38. [CrossRef]
20. So, Y.W.; Chung, G.J.; Ji, W.L. Evaluation of Watershed Scale Aquatic Ecosystem Health by SWAT Modeling and Random Forest Technique. *Sustainability* **2019**, *11*, 3397.
21. Aguilera, R.; Sabater, S.; Marce, R.A. Methodolofical Framwork for Characerizing the Spatiotemporal Variability of River Water-Quality Patterns using Dynamic Factor Analysis. *J. Environ. Inform.* **2018**, *31*, 97–110.
22. Xu, X.; Jiang, Y.; Liu, M.H. Modeling and assessing agro-hydrological processes and irrigation water saving in the middle Heihe River basin. *Agric. Water Manag.* **2019**, *211*, 152–164. [CrossRef]
23. Malagò, A.; Vigiak, O.; Bouraoui, F.; Pagliero, L.; Franchini, M. The Hillslope Length Impact on SWAT Streamflow Prediction in Large Basins. *J. Environ. Inform.* **2018**, *32*, 82–97.
24. Yang, X.K.; Lu, X.X.; Ran, L.S. Geomorphometric Assessment of the Impacts of Dam Construction on River Disconnectivity and Flow Regulation in the Yangtze Basin. *Sustainability* **2019**, *11*, 3427. [CrossRef]
25. Chen, X.J. Modeling hydrodynamics and salt transport in the Alafia River estuary, Florida during May 1999–December 2001. *Estuar. Coast. Shelf Sci.* **2004**, *61*, 477–490. [CrossRef]
26. Ng, S.M.Y.; Wai, O.W.H.; Li, Y.S.; Li, Z.L.; Jiang, Y. Integration of a GIS and a complex three-dimensional hydrodynamic, sediment and heavy metal transport numerical model. *Adv. Eng. Softw.* **2009**, *40*, 391–401. [CrossRef]
27. Long, Y.; Yang, Y.; Lei, X.; Tian, Y.; Li, Y. Integrated assessment method of emergency plan for sudden water pollution accidents based on improved topsis, shannon entropy and a coordinated development degree model. *Sustainability* **2019**, *11*, 510. [CrossRef]
28. Tang, C.H.; Yi, Y.J.; Yang, Z.F. Water pollution risk simulation and prediction in the main canal of the South-to-North Water Transfer Project. *J. Hydrol.* **2014**, *519*, 2111–2120. [CrossRef]
29. Hu, J.; Sun, L.; Li, C.H.; Wang, X.; Jia, X.L.; Cai, Y.P. Water Quality Risk Assessment for the Laoguanhe River of China Using a Stochastic Simulation Method. *J. Environ. Inform.* **2018**, *31*, 123–136. [CrossRef]
30. Adnan, M.S.; Rahmat, S.N.; Tan, L.W.; Rosly, N. Application of SWAT and GIS to simulate the river flow of the Sembrong River, Johor, Malaysia. *Adv. Civ. Archit. Struct. Constr. Eng.* **2016**, *3*, 393–397.
31. Wang, X.H.; Homer, M.; Dyer, S.D.; White-Hull, C.; Du, C. A river water quality model integrated with a web-based geographic information system. *J. Environ. Manag.* **2005**, *75*, 219–228. [CrossRef] [PubMed]
32. Wang, C.; Bi, J.; Ambros, R.B. Development and application of mathematical models to support total maximum daily load for the Taihu Lake's influent rivers, China. *Ecol. Eng.* **2015**, *83*, 258–267. [CrossRef]
33. Zhang, B.; Yang, S.H.; Hao, Q.T. A temporal-spatial simulation and dynamic regulation system of water quality on sudden water pollution accidents. *Mechatron. Eng. Comput. Inf. Technol.* **2014**, *556–562*, 925–928. [CrossRef]
34. Rui, Y.; Shen, D.; Khalid, S. GIS-based emergency response system for sudden water pollution accidents. *Phys. Chem. Earth* **2015**, *79–82*, 115–121. [CrossRef]
35. Portoghese, I.; Uricchio, V.; Vurro, M. A GIS tool for hydrogeological water balance evaluation on a regional scale in semi-arid environments. *Comput. Geosci.* **2005**, *31*, 15–27. [CrossRef]

36. Iqbal, J.; Gorai, A.K.; Katpatal, Y.B.; Pathak, G. Development of GIS-based fuzzy pattern recognition model (modified DRASTIC model) for groundwater vulnerability to pollution assessment. *Int. J. Environ. Sci. Technol.* **2015**, *12*, 3161–3174. [CrossRef]
37. Li, L.Z.; Qian, Y.; Zhang, Y.C. Forecasting and warning the accidental water pollution effect based on the EFAD and WASP. *Resour. Environ. Yangtze Basin* **2011**, *20*, 1010–1016.
38. Zhang, B.; Wang, Q.; Sun, Q.; Li, S. Spatio-temporal simulation of water quality based on SD-GIS accidential water pollution. *Geomatics Inf. Sci. Wuhan Univ.* **2009**, *34*, 348–351.
39. Olivera, F.; Valenzuela, M.; Srinivasan, R.; Choi, J. ArcGIS-SWAT: A geo-data model and GIS interface for SWAT. *J. Am. Water Resour. Assoc.* **2006**, *2*, 295–309. [CrossRef]
40. Zhan, S.P.; Zhou, J.T. Research on visualization of pollution concentration distribution in sea water using GIS. *J. DaLian Univ. Technol.* **2004**, *4*, 506–509.
41. Ding, X.W.; Zhu, Q.; Zai, A.F.; Liu, L. Water quality safety prediction model for drinking water source areas in Three Gorges Reservoir and its application. *Ecol. Indic.* **2019**, *101*, 734–741. [CrossRef]
42. Li, J.X.; Liao, W.G.; Huang, Z.L. Numerical simulation of water quality for the Three Gorges Project Reservoir. *J. Hydraul. Eng.* **2002**, *33*, 7–10.
43. Li, J.X.; Liao, W.G. The effect of water flow on the biodegradation of organic pollution. *Res. Environ. Sci.* **2002**, *15*, 45–48.
44. Peng, Y.; Zhang, H.W.; Zhang, Y. 2D numerical modeling for unsteady flow and sediment transport in Chongqing reach. *J. Hydroelectr. Eng.* **2005**, *24*, 47–52.
45. Xie, Z.T.; Hou, W.G.; Ren, N.H. 2D horizontal modeling for the movement of flow and sediment from Yichang to Yangjianao reach at the Gezhouba downstream. *Adv. Water Sci.* **2008**, *19*, 309–316.
46. Elkady, A.A.; Sweet, S.T.; Wade, T.L.; Klein, A.G. Distribution and assessment of heavy metals in the aquatic environment of Lake Manzala, Egypt. *Ecol. Indic.* **2015**, *58*, 445–457. [CrossRef]
47. Bastami, K.D.; Bagheri, H.; Kheirabadi, V.; Zaferani, G.G.; Teymori, M.B.; Hamzehpoor, A. Distribution and ecological risk assessment of heavy metals in surface sediments along southeast coast of the Caspian Sea. *Mar. Pollut. Bull.* **2014**, *81*, 262–267. [CrossRef]
48. Nazeer, S.; Hashmi, M.Z.; Malik, R.N. Heavy metals distribution, risk assessment and water quality characterization by water quality index of the River Soan, Pakistan. *Ecol. Indic.* **2014**, *43*, 262–270. [CrossRef]
49. Lalit, K.P.; Kumar, D.; Yadav, A.; Rai, J.; Gaur, J.P. Morphological abnormalities in periphytic diatoms as a tool for biomonitoring of heavy metal pollution in a river. *Ecol. Indic.* **2014**, *36*, 272–279.
50. Li, J.; Chen, Z.X. A new stabilized finite volume method for the stationary Stokes equations. *Adv. Comput. Math.* **2009**, *30*, 141–152. [CrossRef]
51. Audusse, E.; Bouchut, F.; Bristeau, M.O.; Klein, R.; Perthame, B. A fast and stable well-balanced scheme with hydrostatic reconstruction for shallow water flows. *SIAM J. Sci. Comput.* **2004**, *25*, 2050–2065. [CrossRef]
52. Qu, Y.Z.; Duffy, C.J. A semidiscrete finite volume formulation for multiprocess watershed simulation. *Water Resour. Res.* **2007**, *43*, 1073–1078. [CrossRef]
53. Hughes, T.J.R.; Cottrell, J.A.; Bazilevs, Y. Isogeometric analysis: CAD, finite elements, NURBS, exact geometry and mesh refinement. *Comput. Methods Appl. Mech. Eng.* **2005**, *194*, 4135–4195. [CrossRef]
54. Zhang, Y.J.; Zhang, Y.H.; Wang, L.J. Application of Emergency Water Environment Risk Area Partitioning in the Three Gorges Reservoir. *Environ. Sci. Technol.* **2015**, *32*, 15–21.
55. Fu, J.C.; Hsu, M.H.; Duann, Y. Development of roughness updating based on artificial neural network in a river hydraulic model for flash flood forecasting. *J. Earth Syst. Sci.* **2016**, *125*, 1–14. [CrossRef]
56. Hou, D.B.; Song, X.X.; Zhang, G.X.; Zhang, H.J. An early warning and control system for urban, drinking water quality protection: China's experience. *Environ. Sci. Pollut. Res.* **2013**, *20*, 4496–4508. [CrossRef]
57. Wu, W.M.; Vieira, D.A.; Wang, S.S.Y. One-dimensional numerical model for nonuniform sediment transport under unsteady flows in channel networks. *J. Hydraul. Eng.* **2004**, *130*, 914–923. [CrossRef]
58. Kumar, M.; Natarajan, G. On the role of discrete mass conservation for non-Boussinesq flow simulations in enclosures. *Int. J. Heat Mass Transf.* **2017**, *104*, 1283–1299. [CrossRef]
59. Qu, Z.G.; Tao, W.Q.; He, Y.L. Implementation of clear algorithm on collocated grid system and application examples. *Numer. Heat Transf. Part B-Fundam.* **2005**, *50*, 73–77. [CrossRef]
60. Gao, Q.; Li, Y.; Cheng, Q.Y.; Yu, M.X.; Hu, B.; Wang, Z.G.; Yu, Z.Q. Analysis and assessment of the nutrients, biochemical indexes and heavy metals in the Three Gorges Reservoir, China, from 2008 to 2013. *Water Res.* **2016**, *92*, 262–274. [CrossRef]

61. Li, L.J.; Deng, P.X. Simulation of water quality variation in middle reaches of Yangtze River before and after operation of Three Gorges Project. *Yangtze River* **2018**, *49*, 51–56.
62. Lei, Y.U.; Hua, G.U.; Lou, C.H.; Wang, G.Q. Simulation of Accidental Water Pollution in Da'ning Reservoir of Beijing South-to-North water diversion project based on MIKE21FM. *South-To-North Water Transf. Water Sci. Technol.* **2013**, *11*, 67–71.